

OPEN ACCESS

Experimental Determination of Si Self-Interstitial Emission During Oxide Precipitation in Czochralski Silicon

To cite this article: G. Kissinger *et al* 2024 *ECS J. Solid State Sci. Technol.* **13** 083005

View the [article online](#) for updates and enhancements.

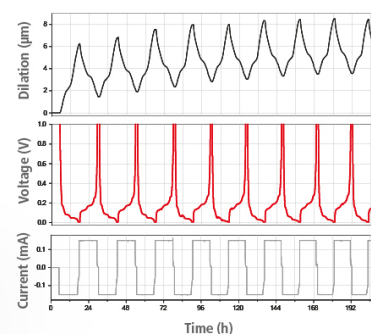
You may also like

- [Carbon in the presence of high oxygen levels in polysilicon: the effect on poly-to-poly dielectric breakdown](#)
Richard F Hafer and T S Moss
- [Sensitivity analyses of furnace material properties in the Czochralski crystal growth method for silicon](#)
O R Asadi Noghabi, M M'Hamdi and M Jomâa
- [The Interrelation Between the Morphology of Oxide Precipitates and the Junction Leakage Current in Czochralski Silicon Crystals](#)
Hiroyuki Fujimori, Yukihiro Ushiku, Toshihiko Ilnuma *et al.*

Watch Your Electrodes Breathe!

Measure the Electrode Expansion in the Nanometer Range with the ECD-4-nano.

- ✓ Battery Test Cell for Dilatometric Analysis (Expansion of Electrodes)
- ✓ Capacitive Displacement Sensor (Range 250 μm , Resolution ≤ 5 nm)
- ✓ Detect Thickness Changes of the Individual Half Cell or the Full Cell
- ✓ Additional Gas Pressure (0 to 3 bar) and Temperature Sensor (-20 to 80° C)



EL-CELL[®]
electrochemical test equipment

See Sample Test Results:



Scan me!

Download the Data Sheet (PDF):



Scan me!

Or contact us directly:

+49 40 79012-734

sales@el-cell.com

www.el-cell.com



Experimental Determination of Si Self-Interstitial Emission During Oxide Precipitation in Czochralski Silicon

G. Kissinger,^{1,z}  D. Kot,¹ and A. Sattler²

¹IHP—Leibniz-Institut für innovative Mikroelektronik, Im Technologiepark 25, 15236 Frankfurt (Oder), Germany

²Siltronic AG, Einsteinstrasse 172, 81677 München, Germany

We used the method of Torigoe and Ono [*J. Appl. Phys.*, **121**, 215103 (2017)] to investigate the kinetics of β , the number of self-interstitials emitted per precipitated oxygen atom, during oxide precipitation in Czochralski silicon. For this purpose, we used pp-epitaxial wafers with a buried highly B-doped epitaxial layer which were annealed with and without thermal pre-treatments at 950 °C. From the results we conclude that in the initial phase of oxide precipitation without thermal pre-treatment β is very high before it drops to low values. With a thermal pre-treatment at 800 °C for 2 h, the initial value of β is somewhat lower before the drop also occurs. If a nucleation anneal is carried out before the thermal treatment at 950 °C the β values are low from the beginning. All of these results confirm our previously published theoretical predictions experimentally. This work also shows that the crystal pulling process can affect the initial β value because grown-in oxide precipitate nuclei can reduce their strain by vacancy absorption. Therefore, high vacancy supersaturation during crystal cooling while oxide precipitate nucleate would lead to somewhat lower initial β values.

© 2024 The Author(s). Published on behalf of The Electrochemical Society by IOP Publishing Limited. This is an open access article distributed under the terms of the Creative Commons Attribution 4.0 License (CC BY, <http://creativecommons.org/licenses/by/4.0/>), which permits unrestricted reuse of the work in any medium, provided the original work is properly cited. [DOI: 10.1149/2162-8777/ad670d]



Manuscript submitted June 27, 2024; revised manuscript received July 24, 2024. Published August 13, 2024.

Controlling oxide precipitation in silicon during thermal processing is still very important because oxide precipitates can be harmful as well as beneficial to electronic devices. Placed in the device active zone below the surface of silicon wafers, they can degrade the device function, cause early breakdowns of gate oxides, or even cause shorts.^{1–4} In the bulk of silicon wafers, oxide precipitates can serve as gettering sinks for accidentally introduced metallic impurities, which otherwise can degrade the device function.^{3,5–7} However, the density of oxide precipitates in the bulk of silicon wafers must be carefully controlled because in too high density they could cause deformations of the large silicon wafers leading to overlay problems in photolithography.^{1,8} Controlling oxide precipitation also means that size and density can be predicted as accurate as possible by simulation models. There are many influencing factors and still open issues which should be elucidated to improve the accuracy of simulation.

One of these open issues is the number β of silicon self-interstitials emitted per precipitated oxygen atom. Self-interstitials are emitted to relieve the strain caused by the difference in the molecular volumes of silicon and the silicon oxide SiO_x of the precipitate.⁹ The value of β impacts among others the growth rate of oxide precipitates.¹⁰ It was already found that β is temperature dependent.¹¹ In a theoretical work, we demonstrated that in the initial stage of oxide precipitation β is very high and then suddenly drops to low values with a simultaneous change of the stoichiometry x of the precipitated oxide.¹² The critical number of oxygen atoms in the precipitates when the drop takes place depends on both the precipitate density and the temperature of annealing.¹²

In an experimental work, Torigoe et al.¹¹ showed that it is possible to use interstitial enhanced diffusion of boron in p/p+ epitaxial wafers to determine β . They determined time averaged values for β as function of temperature in the range from 850 °C to 1000 °C and demonstrated that β is decreasing with decreasing temperature of annealing. However, they did not determine the kinetics of β .

In this work, we used the method of Torigoe et al.¹¹ to investigate the kinetics of β . We carefully chose the material to be able to detect if the drop of β really exists. This drop is important because it coincides with important features of oxide precipitates like getter efficiency and degradation of the lifetime of minority carriers.¹² The most suitable silicon material for our investigation should have a moderate density of oxide precipitates and the anneal temperature should be as high as possible so that the equilibrium precipitate morphology is still plate-like. These conditions are best fulfilled for

pp- epitaxial wafers and annealing at 950 °C. Higher anneal temperatures would be even better but precipitate morphology would change to octahedral.^{13,14}

Experimental

Two types of N co-doped Czochralski silicon wafers were used as substrates for epitaxy. The first type are Ultimate Silicon™ wafers from crystals grown in the Pv-region, the second type was produced from fast pulled silicon crystals containing voids. Both wafer types were 300 mm in diameter and B-doped with a resistivity of about 10 Ωcm , corresponding to a B concentration C_B of about $1 \times 10^{15} \text{cm}^{-3}$. The initial concentrations of interstitial oxygen $C_{O_i}^0$, determined by Fourier transform infrared spectrometry (FTIR), were $5.9 \times 10^{17} \text{cm}^{-3}$ and $5.3 \times 10^{17} \text{cm}^{-3}$ (conversion factor $2.45 \times 10^{17} \text{cm}^{-2}$) for the Ultimate™ and COP-rich wafers, respectively.

On the substrate wafers, 3 μm highly B-doped silicon ($C_B = 1 \times 10^{17} \text{cm}^{-3}$) followed by 12 μm moderately B-doped silicon ($C_B = 1 \times 10^{13} \text{cm}^{-3}$) were deposited epitaxially. From the center of the p/p- epitaxial wafers 5 cm \times 5 cm samples were cut. In the next step, one group of the p/p- samples received a nucleation anneal of 32 h at 650 °C to generate a high density of oxide precipitate nuclei in the substrate followed by 800 °C for 2 h to stabilize the precipitate nuclei. Another group of samples received only the stabilization treatment of 800 °C for 2 h. A third group of samples was not pre-treated at all. Then, all samples were annealed for either 4 h, 12 h, 24 h, or 48 h at 950 °C. Table I provides an overview of the applied treatments. All anneals were carried out in nitrogen atmosphere.

For the measurements to be carried out on each of the samples, these were further cut into 4 samples of 2.5 cm \times 2.5 cm size, one for secondary ion mass spectrometry (SIMS) measurement of the B-profile, one for measurement of the BMD density, one for measurement of the loss of interstitial oxygen by FTIR and a spare one. The SIMS measurements of the B profiles were carried out by SGS Institute Fresenius GmbH in Dresden using a Cameca IMS 7 F SIMS tool. The depth profiles of up to 20 μm depth were acquired by sputtering with a Cs^+ ion beam with an energy of 15 keV over a $130 \times 130 \mu\text{m}^2$ area. The masses of $^{28}\text{Si}^{10}\text{B}$, $^{28}\text{Si}^{11}\text{B}$, and $^{30}\text{Si}_2$ were analyzed over a $\varnothing 70 \mu\text{m}$ area in the center of the crater produced by the cesium beam. The concentrations were quantified using a reference implantation of boron in silicon. The depth axis was calibrated by measuring the crater depths. Reference profiles of each wafer type were also measured using epitaxial wafers without any thermal treatment.

^zE-mail: gudrun.kissinger@magenta.de

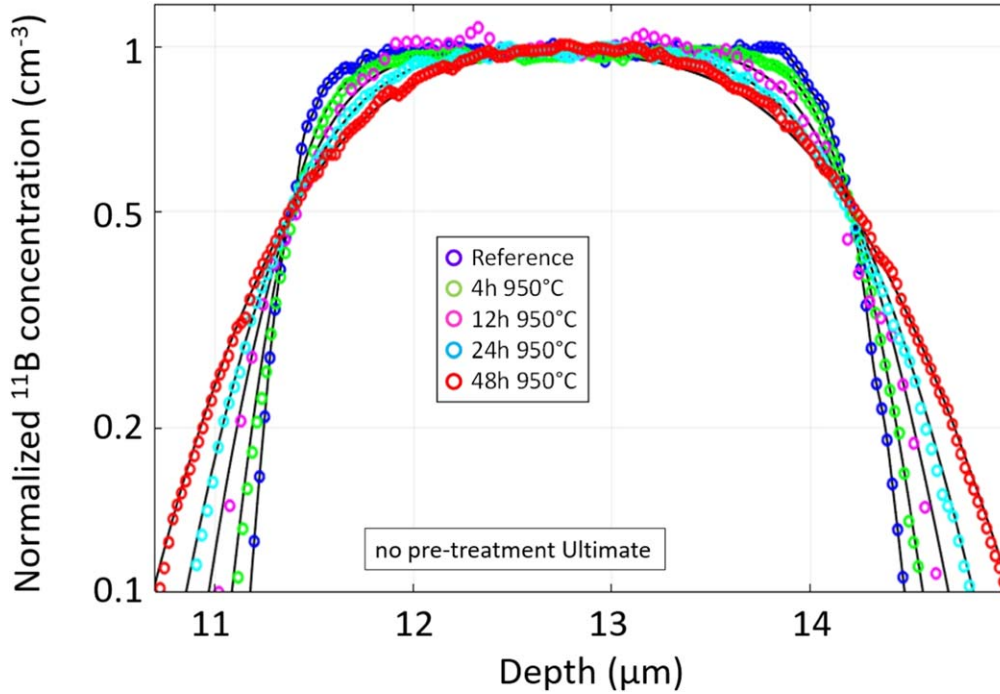


Figure 1. Experimental values of the normalized B concentration plotted as a function of depth (symbols) and the corresponding simulated B profiles (black lines) both for Ultimate samples without pre-treatment.

Table I. Substrate materials and thermal treatments applied to epitaxial wafers.

Substrate wafer type	Pre-treatment		Anneal			
	32 h 650 °C	800 °C 2 h	950 °C 4 h	950 °C 12 h	950 °C 24 h	950 °C 48 h
Ultimate	—	—	X	X	X	X
Ultimate	—	X	X	—	X	X
Ultimate	X	X	X	—	X	X
V-rich	—	—	X	X	X	X

For fitting simulated B profiles to experimental B profiles, it is important to determine the bulk microdefect (BMD) density as accurate as possible because the simulation results are very sensitive to the BMD density used. The BMD densities N_{BMD} used for simulation were determined by Secco etching¹⁵ of a (110) cleavage plane perpendicular to the wafer surface. For measurement, the samples with the longest annealing times were used because for shorter annealing times some of the oxide precipitate nuclei may have not passed the detection limit. It was found that the BMDs are distributed very homogeneously in the depth of the samples. Below the surface, a defect denuded zone (DZ) exists which was also measured. All measured values can be found in Table II.

Scanning transmission electron microscopy (STEM) was used to investigate the morphology and size of oxide precipitates of selected samples. For this purpose, an FEI Tecnai Osiris tool was used.

Modelling

The aim of modelling is to determine the number of silicon self-interstitials emitted per precipitated oxygen atom β . For this purpose, simulated B profiles are fitted to the experimental profiles, measured by SIMS. Modelling exploits the phenomenon of interstitial enhanced B diffusion (see e.g. 16–18) and for simulation of the boron profiles the one-dimensional diffusion equation according to Fick's second law of diffusion has to be solved. Our model is based on the model of Torigoe et al.¹¹ with a few slight deviations mentioned below. It is assumed that the effective diffusivity of B is determined by diffusion via self-interstitials. The contribution of vacancies is neglected. Then, the diffusion equation to be solved reads

$$\frac{\partial C_B}{\partial t} = \frac{\partial}{\partial x} \left(D_B^* \frac{C_I}{C_I^{eq}} \frac{\partial C_B}{\partial x} \right). \quad [1]$$

Here, C_B , C_I , and C_I^{eq} are the B concentration, the silicon self-interstitial concentration, and the thermal equilibrium concentration of self-interstitials, respectively. The diffusivity D_B^* is the diffusivity of B under thermal equilibrium conditions of self-interstitials and vacancies. We determined D_B^* from the values published by Torigoe

Table II. BMD densities and depths of the defect denuded zones measured after Secco etching and used for simulation.

Substrate wafer type	Pre-treatment	N_{BMD} (cm ⁻³)	Depth of DZ (μm)	$C_{O_i}^0$ (cm ⁻³)
Ultimate	no	9.0×10^8	11.6	5.9×10^{17}
Ultimate	800 °C 2 h	9.0×10^8		5.9×10^{17}
Ultimate	650 °C 32 h + 800 °C 2 h	3.4×10^{10}	6.8	5.9×10^{17}
V-rich	no	1.05×10^9	4.5	5.3×10^{17}

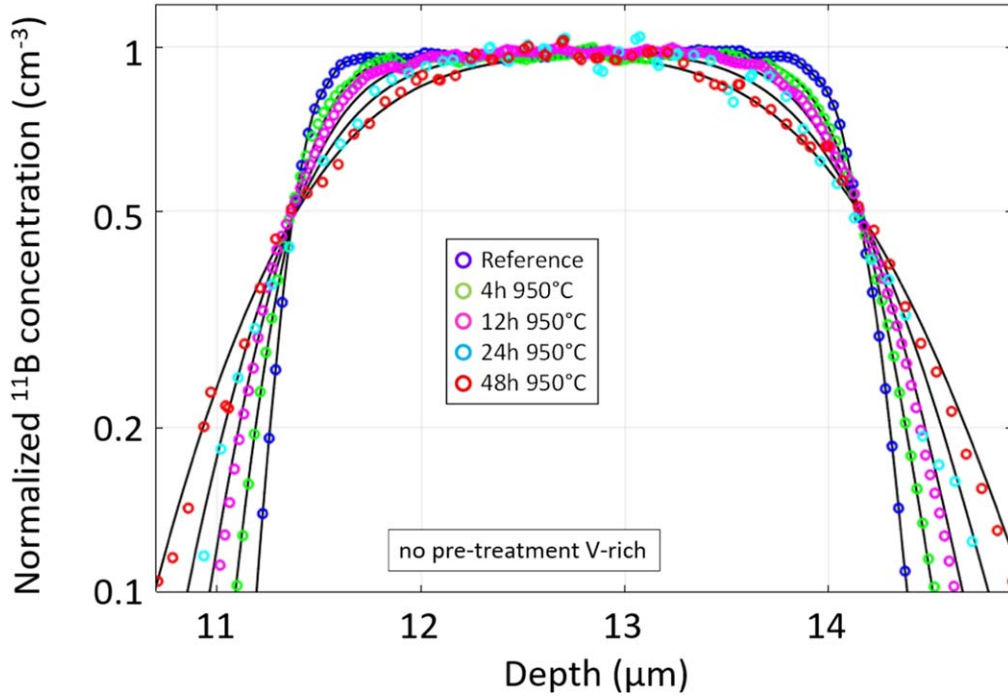


Figure 2. Experimental values of the normalized B concentration plotted as a function of depth (symbols) and the corresponding simulated B profiles (black lines) both for V-rich samples without pre-treatment.

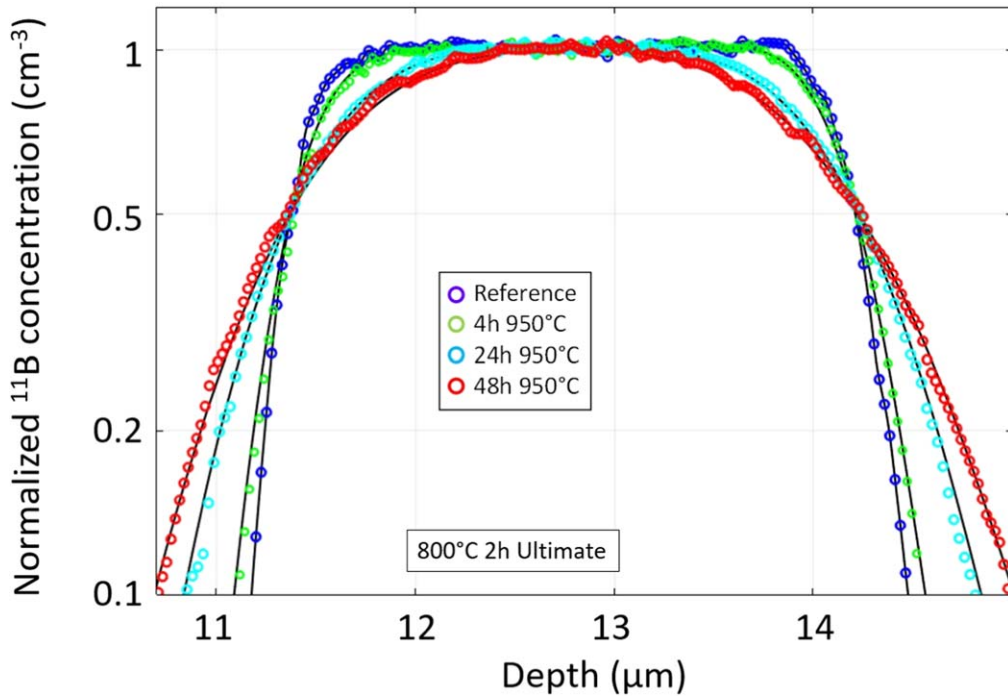


Figure 3. Experimental values of the normalized B concentration plotted as a function of depth (symbols) and the corresponding simulated B profiles (black lines) both for Ultimate samples with pre-treatment at 800 °C for 2 h.

et al. in Ref. 11. The B profiles of the reference samples served as the initial values of C_B .

The boron profiles are affected by different sources and sinks of self-interstitials. The growing oxide precipitates emit self-interstitials to relieve part of the strain resulting from the volume difference between the silicon matrix and the silicon oxide precipitates. The number of interstitials emitted per precipitated oxygen atom β is the fitting parameter which we finally wanted to determine. During

growth, the increasing strain can be also relieved by generation of secondary defects, i.e. mostly dislocation loops. Self-interstitials emitted by the precipitate can be absorbed by the dislocations. The change of C_I with time t can be described as follows

$$\frac{\partial C_I}{\partial t} = \frac{\partial}{\partial x} \left(D_I \frac{\partial C_I}{\partial x} \right) + 4\pi\beta R D_{O_i}^{eff} \cdot 2.088 \cdot (C_{O_i} - C_{O_i}^{if}) \cdot N_{BMD} - 2\pi r_{core} L D_I (C_I - C_I^{eq}) N_{BMD} / \lambda \quad [2]$$

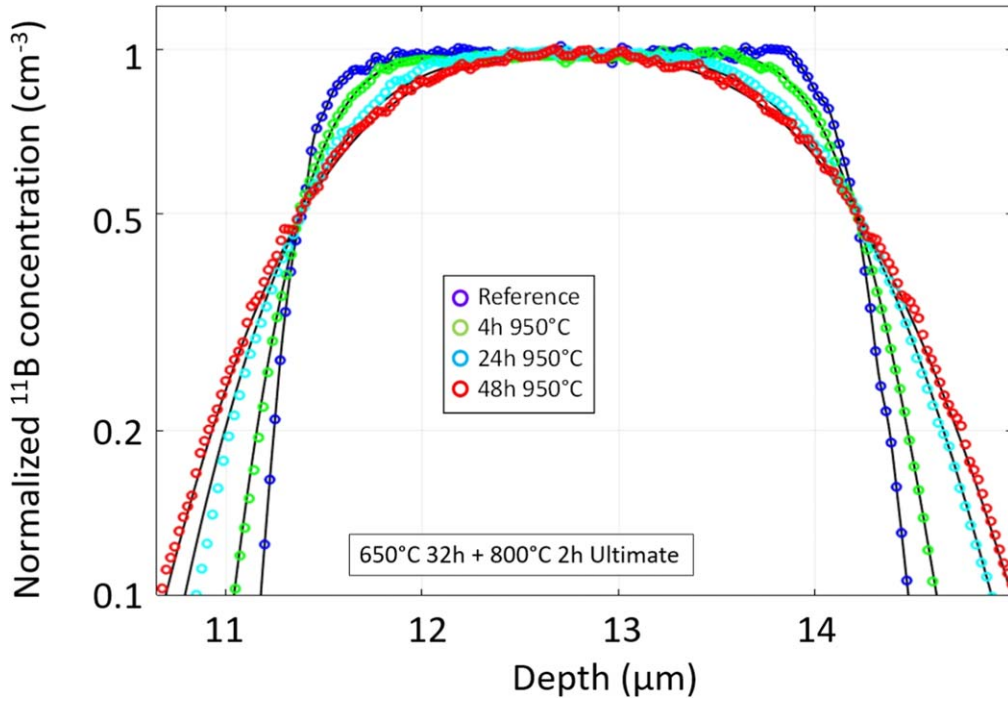


Figure 4. Experimental values of the normalized B concentration plotted as a function of depth (symbols) and the corresponding simulated B profiles (black lines) both for Ultimate samples with pre-treatment at 650 °C for 32 h + 800 °C for 2 h.

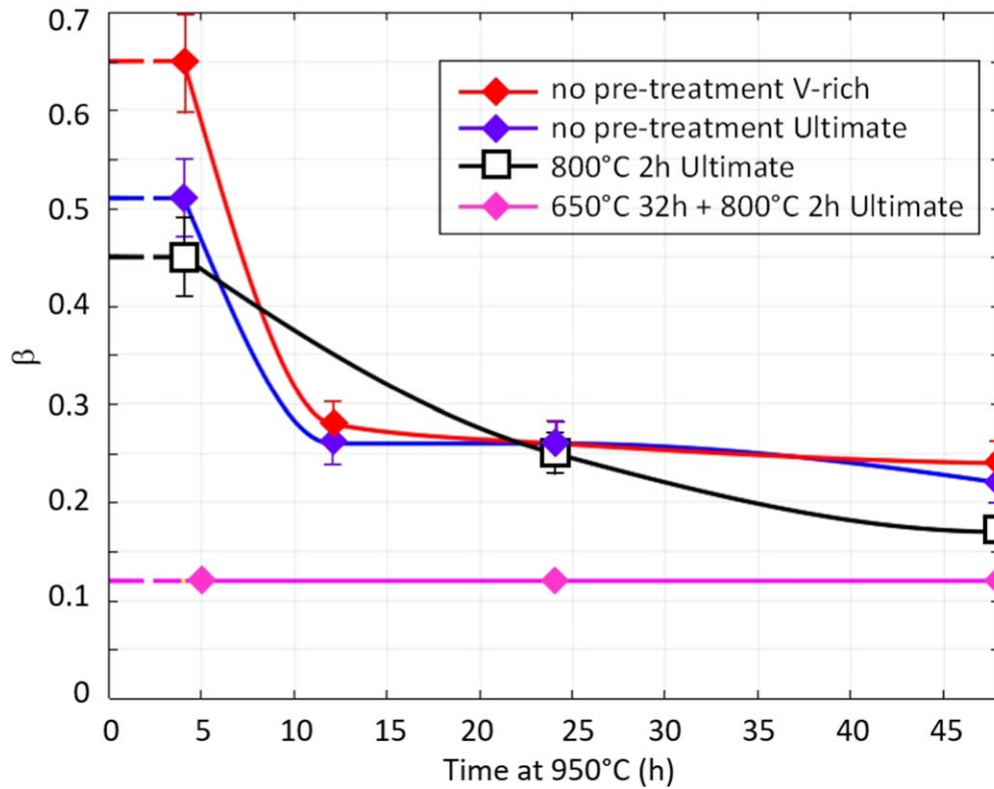


Figure 5. Function $\beta(t)$ determined for the different wafer types.

where the first term represents the diffusion of self-interstitials, the second term represents the emission of self-interstitials from growing oxide precipitates, and the third term stands for the absorption of self-interstitials at secondary dislocations. The latter

one is based on empirical expressions and extensively described in Ref. 11. The radius of the dislocation core is assumed to be $r_{core} = 0.5$ nm and L and λ are represented by empirical equations from Refs. 11, 19 as follows

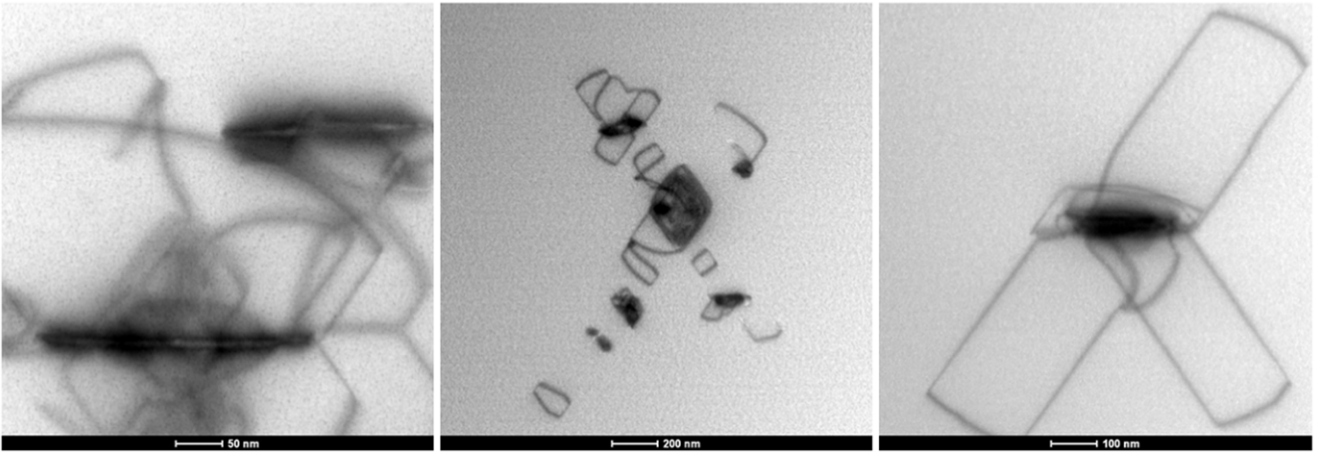


Figure 6. STEM images of plate-like oxide precipitates surrounded by secondary dislocations observed in samples from the Ultimate wafer annealed at 950 °C for 24 h (left), the V-rich wafer annealed at 950 °C for 24 h (middle), and the Ultimate wafer annealed 650 °C 32 h + 800 °C 2 h + 950 °C 24 h (right).

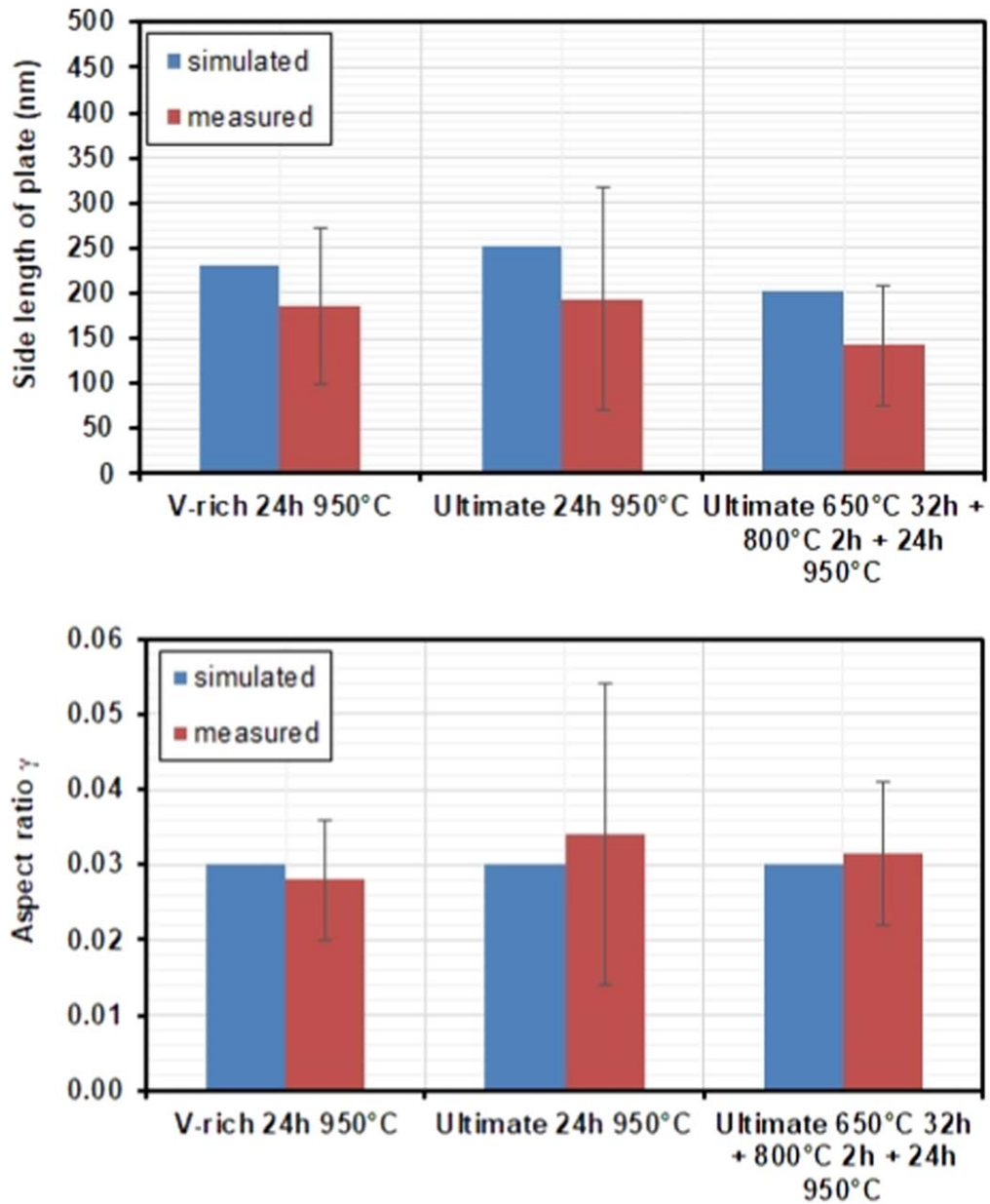


Figure 7. Side length (above) and aspect ratio γ (below) of plate-like precipitates observed by STEM in different samples.

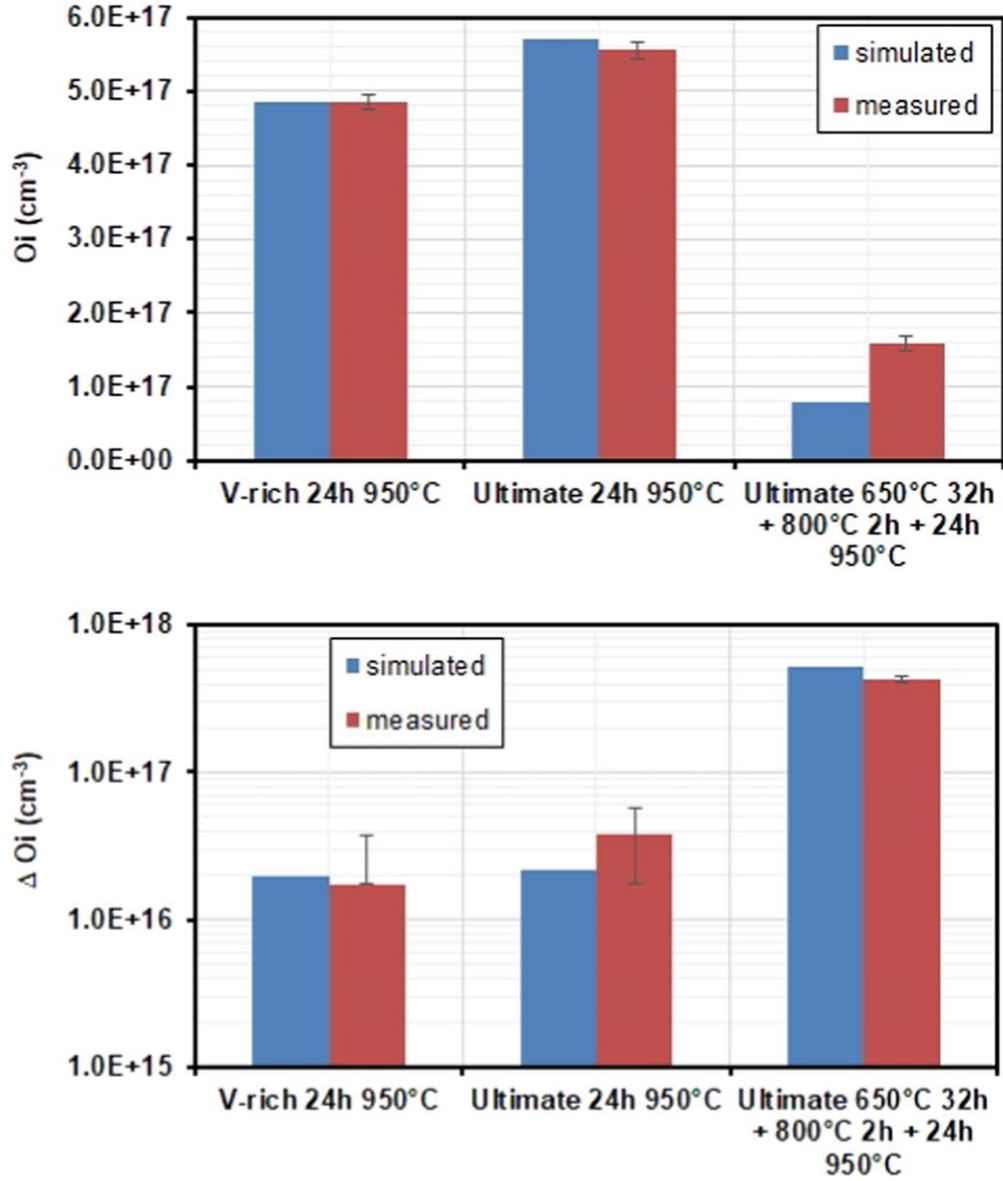


Figure 8. Concentration of interstitial oxygen O_i (above) and loss of interstitial oxygen ΔO_i (below) of plate-like precipitates observed by STEM in different samples.

$$\lambda = 1.4 \times 10^{-3} L^{0.47} \text{ (cm)} \quad [3]$$

$$L = 2.82 \times 10^{14} R^{3.35} \text{ (cm)}. \quad [4]$$

In Eq. 2, D_I represents the diffusivity of self-interstitials and $C_{O_i}^{if}$, the concentration of interstitial oxygen at the interface oxide precipitate/silicon matrix, was assumed to correspond to the solubility of interstitial oxygen. The radius R is the radius of a spherical oxide precipitate with the same volume as a plate-like precipitate. The change of R with t can be obtained via

$$\frac{\partial R}{\partial t} = \frac{D_{O_i}^{eff}}{R} \cdot \frac{\sqrt{1-\gamma^2}}{\gamma^{1/3} \arccos \gamma} \cdot \frac{(C_{O_i} - C_{O_i}^{if})}{C_P}. \quad [5]$$

The middle term is a geometric factor, being larger than 1, which describes the influence of the aspect ratio of a plate-like precipitate on the growth rate with γ being the aspect ratio of the platelet.²⁰

Applying an aspect ratio $\gamma = 0.03$ as determined by Sueoka et al. on p/p+ epitaxial wafers,²¹ the value of the middle term amounts to 2.088. The geometric factor in Ref. 11 does not fulfill the criterion of being larger than 1. For this reason, it was replaced by the factor from Ref. 20. The concentration of O in the oxide precipitate, assuming SiO_2 , amounts to $C_P = 4.52 \times 10^{22} \text{ cm}^{-3}$. According to Torigoe et al.,²² the effective diffusivity of interstitial oxygen depends on the boron concentration and can be obtained as follows

$$D_{O_i}^{eff} = D_{O_i} + (3.3 \pm 0.8) \times 10^{-35} C_B^{0.5} \times C_{O_i} \exp \left[\frac{-(1.1 \pm 0.05) eV}{kT} \right] \text{ cm}^2 \text{ s}^{-1}. \quad [6]$$

The diffusivity D_I and solubility C_I^{eq} of self-interstitials were taken from Frewen et al.²³ and diffusivity D_{O_i} and solubility $C_{O_i}^{eq}$ of interstitial oxygen both stem from Mikkelsen.²⁴

A few changes with respect to Torigoe's model¹¹ were taken. We omitted the Gibbs-Thomson effect because it affects only very small oxide precipitates which play a negligible role in our case because

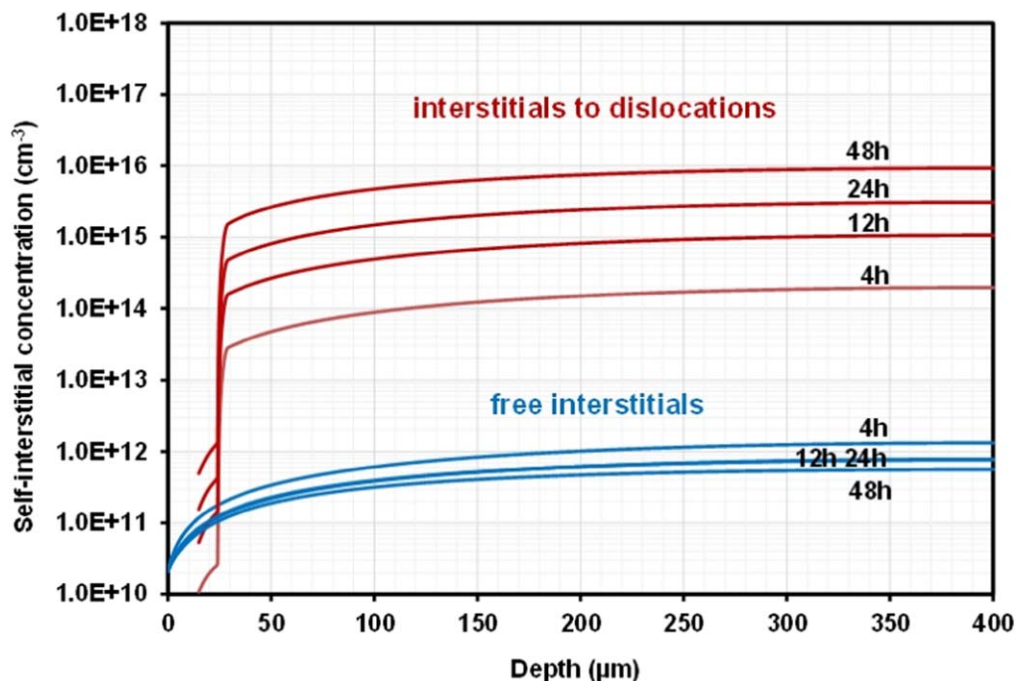


Figure 9. Free self-interstitials and self-interstitials absorbed by dislocations plotted as function of the wafer depth for different annealing times at 950 °C for Ultimate samples without pre-treatment.

during epitaxy the oxide precipitates are already grown to a simulated size of 10 nm used as the initial radius. Only in case of annealing 32 h at 650 °C + 2 h at 800 °C, we used an initial radius of 0.5 nm for the new precipitate nuclei.

Solving Eqs. 1, 2 and 5 and using β as a fit parameter the B profiles can be simulated. The boundary conditions at both surfaces are zero flux conditions. Only for C_{O_i} and C_I Dirichlet boundary conditions are assumed with $C_{O_i} = 0$ and $C_I = C_I^{eq}$. In the first run, we determined a constant β for each sample. Starting with these values, a time dependent β function $\beta(t)$ was determined for each wafer type in the second run.

Results and Discussion

Figures 1–4 show the experimental and the corresponding simulated B profiles using a $\beta(t)$ function for each wafer type. It can be seen that it is possible to fit all experimental B profiles of a wafer type with one $\beta(t)$ function.

In Fig. 5, the $\beta(t)$ functions of the different sample types are compared. Samples without pre-anneal exhibit high β values for short annealing times which then drop to nearly the same low β values for prolonged annealing. This is in very good agreement with the theoretical results in Ref. 12 which predict a high β for very small sizes of oxide precipitates and a sudden drop to very low values if a critical size is reached. If we compare the high initial β values for the Ultimate and V-rich samples without pre-anneal, we can see that the V-rich sample exhibits the highest initial β value. In contrast to the Ultimate sample, this sample contains a relatively high concentration of voids, approximately $5 \times 10^5 \text{ cm}^{-3}$ to $1 \times 10^7 \text{ cm}^{-3}$. During the crystal pulling process, these voids reduced the vacancy supersaturation before oxide precipitate nucleation started. The Ultimate crystals were grown in the Pv-region meaning their vacancy supersaturation was higher and the oxide precipitate nuclei could relief their strain more efficiently by vacancy absorption. This would explain the lower initial β values for the Ultimate samples because lower strain requires less emission of self-interstitials. For longer annealing times, the effect vanishes because the number of precipitated oxygen atoms becomes large relative to the space provided by the absorbed

vacancies. Therefore, prolonged annealing results in similar β values for all sample types without pre-anneal.

The samples with nucleation anneal 650 °C for 32 h behave completely different. Their $\beta(t)$ functions exhibit only constantly low β values. This behavior is also well in agreement with the theoretical predictions in Ref. 12 because at such low temperatures like 650 °C and the two orders of magnitude higher BMD density the drop of β occurs already for very small sizes of oxide precipitates and the β values reached can be assumed to be already very low before the subsequent anneals at 800 °C and 950 °C start.

The $\beta(t)$ function of the samples with pre-anneal at 800 °C for 2 h is difficult to interpret because of the unavailable value of 12 h annealing at 950 °C where a drop of β is very likely but not proven. Nevertheless, it is certain that the initial β value is somewhat lower than for wafers without pre-anneal. This lower initial β value for samples pre-annealed at 800 °C can be assumed to be due to the pre-treatment at a temperature lower than the 950 °C anneal because according to Ref. 12 the initial high β values decrease with temperature. Further conclusions are omitted because these would require an additional data point of 12 h annealing at 950 °C.

We also investigated the morphology of the oxide precipitates in selected samples. Figure 6 provides a few examples of the oxide precipitates which were found to be plate-like and surrounded by secondary dislocations as assumed in the simulation. The side length and aspect ratio, shown in Fig. 7, are in an acceptable agreement with the simulated results.

If we compare the concentrations of interstitial oxygen measured and simulated at the end of all thermal treatments at selected samples they are also in an acceptable agreement as demonstrated in Fig. 8. The same holds for the loss of interstitial oxygen ΔO_i .

Figures 9 and 10 show the self-interstitial distribution between free interstitials and interstitials absorbed by dislocations. The results for samples without pre-annealing and samples pre-annealed at 800 °C are very similar. Therefore we provide only the example in Fig. 9. It can be seen that for samples with nucleation pre-treatment 650 °C 32 h + 800 °C 2 h much more self-interstitials were generated due to the markedly higher BMD density. In all cases, the vast majority of self-interstitials emitted by the growing oxide

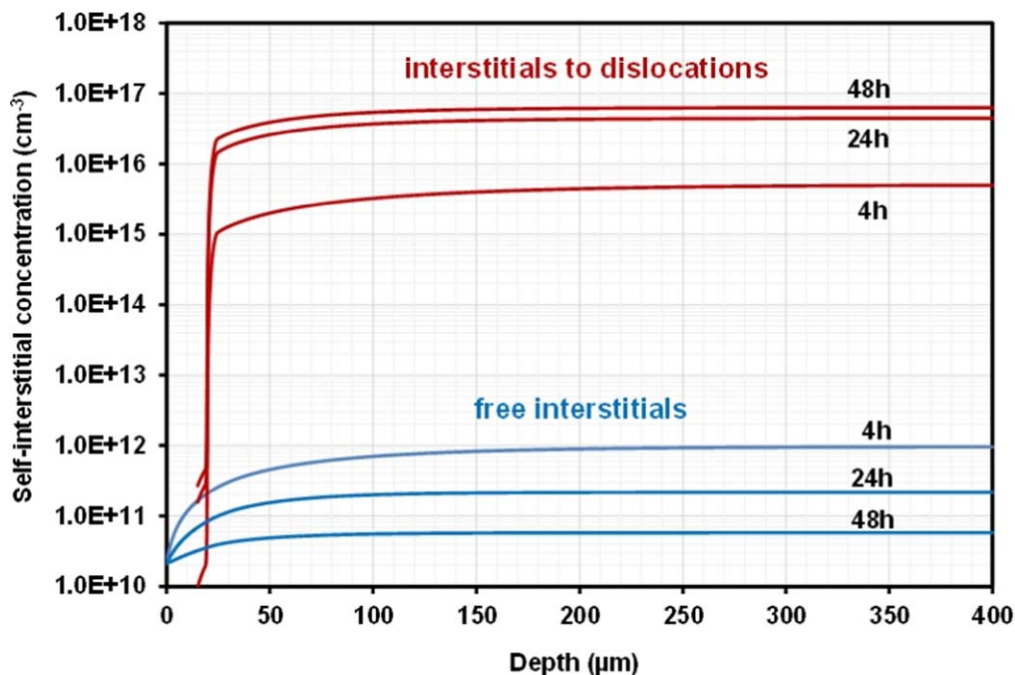


Figure 10. Free self-interstitials and self-interstitials absorbed by dislocations plotted as function of the wafer depth for different annealing times at 950 °C for Ultimate samples with pre-treatment at 650 °C for 32 h + 800 °C for 2 h.

precipitates are absorbed by the secondary dislocations. This result is in very good agreement with the results presented in Ref. 11.

Conclusions

We used the method of Torigoe et al.¹¹ to investigate the kinetics of β , the number of self-interstitials emitted per precipitated oxygen atom, during oxide precipitation in Czochralski silicon. For this purpose, we used pp- epitaxial wafers with a buried highly B-doped epitaxial layer. These were annealed with and without thermal pre-treatment at 950 °C.

From the results, we can conclude that in the initial phase of oxide precipitation without thermal pre-treatment β is very high before it drops to low values. With a thermal pre-treatment at 800 °C for 2 h, the initial value of β is somewhat lower. If a nucleation anneal is carried out before the thermal treatment at 950 °C the β values are very low from the beginning because the drop occurred already during the nucleation anneal. All these results confirm our theoretical predictions in Ref. 12 and the existence of the drop of β experimentally.

It can be further concluded from the results of this work that the crystal pulling process can affect the initial β value because grown-in oxide precipitate nuclei can reduce their strain by vacancy absorption. For this reason, high vacancy supersaturation during crystal cooling while oxide precipitates nucleate would lead to somewhat lower initial β values.

Acknowledgments

The authors would like to thank Dr Thomas Stettner for depositing the epitaxial layers.

ORCID

G. Kissinger  <https://orcid.org/0000-0002-6492-3117>

References

1. Y. Hirano, K. Yamazaki, F. Inoue, K. Imaoka, K. Tanahashi, and H. Yamada-Kaneta, *J. Electrochem. Soc.*, **154**, H1027 (2007).
2. E. Simoen, C. Claeys, and J. Vanhellemont, *Defect and Diffusion Forum*, **261-262**, 1 (2007).
3. R. Hölzl, A. Huber, L. Fabry, K.—J. Range, and M. Blietz, *Appl. Phys. A*, **72**, 351 (2001).
4. T. Tsuya, ed. F. Shimura *Semicond. Semimet.* (1994), Vol. 42(Academic, New York).
5. J. E. Lawrence and H. R. Huff, "Silicon material properties for VLSI circuitry.", ed. N. G. Einspruch *VLSI Electronics: Microstructure Science* 5, 51(Academic, New York) (1982).
6. H. Richter, "Gettering in the silicon device technology - an overview." *Proceedings 1st International Autumn School Gettering and Defect Engineering in the Semiconductor Technology (GADEST), 8–18 Oct 1985, GDR, Garzau1* (1985).
7. S. Takasu, "VLSI science and technology/1984.", ed. K. E. Bean and G. A. Rozgonyi *The Electrochemical Society Proceedings* 84–7, 490(The Electrochemical Society, Pennington) (1984).
8. K. Izunome, *Proc. of the 6th International Symp. on Advanced Science and Technology of Silicon Materials (JSPS Symposium), Kona, 20129* (2012).
9. J. Vanhellemont and C. Claeys, "*J. Appl. Phys.*, **62**, 3960 (1987), Erratum." *J. Appl. Phys.*, **71**, 1073 (1992).
10. G. Kissinger, ed. Y. Yoshida and G. Langouche *Defects and Impurities in Silicon Materials, Lecture Notes in Physics* (2015), Vol. 916(Springer, Japan).
11. K. Torigoe and T. Ono, *J. Appl. Phys.*, **121**, 215103 (2017).
12. G. Kissinger, D. Kot, A. Huber, R. Kretschmer, T. Müller, and A. Sattler, *ECS J. Solid State Sci. Technol.*, **9**, 064002 (2020).
13. H. Fujimori, *J. Electrochem. Soc.*, **144**, 3180 (1997).
14. D. Kot, G. Kissinger, M. A. Schubert, and A. Sattler, *ECS J. Solid State Sci. Technol.*, **3**, P370 (2014).
15. S. d'Aragona, *J. Electrochem. Soc.*, **199**, 948 (1972).
16. D. A. Antoniadis and I. Moskowitz, *J. Appl. Phys.*, **53**, 6788 (1982).
17. P. M. Fahey, P. B. Griffin, and J. D. Plummer, *Rev. Mod. Phys.*, **61**, 289 (1989).
18. H.-J. Gossmann, C. S. Rafferty, H. S. Luftman, F. C. Unterwald, T. Boone, and J. M. Poate, *Appl. Phys. Lett.*, **63**, 639 (1993).
19. K. Torigoe, private communication.
20. Y. Yang, A. Sattler, and T. Sinno, *J. Appl. Phys.*, **125**, 165705 (2019).
21. K. Sueoka, M. Akatsuka, M. Yonemura, T. Ono, E. Asayama, and H. Katahama, *J. Electrochem. Soc.*, **147**, 756 (2000).
22. K. Torigoe, J. Fujise, T. Ono, and K. Nakamura, *J. Appl. Phys.*, **116**, 193503 (2014).
23. T. A. Frewen and T. Sinno, *Appl. Phys. Lett.*, **89**, 191903 (2006).
24. J. C. Mikkelsen Jr, *Mater. Res. Soc. Symp. Proc.*, **59**, 19 (1986).